Clusters binding to the graphene moiré on Ir(111): X-ray photoemission compared to density functional calculations

Jan Knudsen,[1,*] Peter J. Feibelman,[2] Timm Gerber,[3] Elin Grånäs,[1] Karina Schulte,[4] Patrick Stratmann,[3] Jesper N. Andersen,[1] and Thomas Michely[3]

[1]*Division of Synchrotron Radiation Research, Lund University, Box 118, SE-221 00, Sweden*

[2]*Sandia National Laboratories, Albuquerque, New Mexico 87185-1415, USA*

[3]*II. Physikalisches Institut, Universität zu Köln, D-50937 Köln, Germany*

[4]*MAX IV Laboratory, Lund University, Box 118, SE-22100 Lund, Sweden*

(Received 7 July 2011; revised manuscript received 28 November 2011; published 6 January 2012)

Our understanding of metal-atom cluster adsorption on graphene on Ir(111) is based on elementary chemical ideas, rehybridization, and buckling, supported by density functional theory (DFT) calculations. We tested the DFT picture by comparing calculated core level spectra to x-ray photoemission spectroscopy (XPS) measurements. For pristine graphene, which forms a gently undulating moiré on Ir(111), DFT predicts a 140 meV modulation of C 1*s* core level shifts (CLS), consistent with the measured spectrum. With Pt clusters adsorbed, measured Pt 4*f* CLS of the adsorbed clusters also support the calculations. The modulation of the C 1*s* spectrum is strengthened with clusters adsorbed, and C-atom ionization potentials under and in the vicinity of the Pt clusters are shifted enough to be experimentally distinguished as a broad shoulder of positive C 1*s* CLSs. Furthermore, DFT calculations imply that sp^2 to sp^3 graphene rehybridization of C atoms below the Pt cluster induces a 1.1 eV CLS splitting between Pt- and Ir-bonded C atoms; this prediction is also consistent with the XPS data.

DOI: 10.1103/PhysRevB.85.035407 PACS number(s): 79.60.Jv, 61.46.−w, 61.48.Gh, 71.15.Mb

I. INTRODUCTION

Graphene moirés on close-packed noble metal surfaces have become popular substrates for patterned growth of metal clusters and patterned adsorption of gas atoms and organic molecules. Examples include Pt and other metal clusters on the graphene/Ru(0001) moiré,[1–3] Ni clusters on the graphene/Rh(111) moiré,[4] and a variety of metallic and bimetallic clusters[5,6] of hydrogen[7,8] and of organic molecules on graphene/Ir(111).[9] Of these, graphene/Ir(111) induces adcluster arrays whose exceptional order and narrow size distribution makes them particularly attractive laboratories for fundamental studies of nanomagnetism and catalysis.

Unavoidably, the first step toward exploiting this opportunity is to understand the physical chemistry underlying graphene moiré templating—and an appealing interpretation of it has emerged from density functional theory (DFT) calculations for the graphene/Ir(111) moiré. The idea is that beneath and in the vicinity of adsorbed metal clusters,[10,11] the carbon layer rehybridizes from the sp^2 bonding characteristic of graphene to diamondlike sp^3. The sp^3 hybridized carbon atoms then bind with their fourth bond normal to the average carbon plane alternately to substrate Ir atoms directly below or metal atoms directly above. Because such rehybridization is only energetically profitable where there are substrate atoms directly below C atoms, this concept provides a natural explanation for cluster binding only in particular regions of the moiré unit cell. It also lays the groundwork for an important structural test: Specifically, in the DFT calculations the chemical bonds that form between carbon and metal atoms significantly reduce the C atom height above the Ir surface plane from ≈3.4 Å to ≈2.1 Å. Based on DFT calculations, a similar scenario has been proposed for patterned hydrogen adsorption on the graphene/Ir(111) moiré.[7,8]

Despite its plausibility, there is as yet no experimental evidence for the rehybridization picture beyond agreement of the experimentally determined binding site preference of the metal clusters with what DFT calculations predict. A way to proceed is suggested by previous investigations of the binding of graphene to different metals[12,13] and of how differently sized graphene flakes bind to the Ir(111) substrate.[14] In particular, we have acquired x-ray photoelectron spectroscopy (XPS) C 1*s* core level shifts for graphene/Ir(111) carbon atoms with and without adsorbed clusters present, and herein we compare them to calculated shifts based on the rehybridization picture. This is an indispensable test of DFT's predictive capability not just for graphene on a metal and for static metal cluster arrays, but for more complex situations involving chemistry upon them. Such a test appears all the more necessary as recently the DFT interpretation of the corrugation within the moiré unit cell of graphene on Ir(111) was challenged in a report of new atomic force microscopy measurements.[15]

The manuscript is organized as follows: In Sec. II, we report the details of our experimental and calculation methods. In Sec. III, to set a standard for agreement between DFT theory and XPS data, we compare measured and calculated C 1*s* CLS of graphene on Ir(111) without adclusters. The effects of cluster adsorption are the subject of Secs. IV and V, wherein we analyze our experimental and calculated results for the C 1*s* CLS of graphene with Pt adsorbed and for the Pt 4$f_{7/2}$ CLS of the adsorbed clusters themselves.

II. METHODS OF EXPERIMENT AND CALCULATION

XPS experiments were conducted at Beamline I311[16] at the MAX IV Laboratory in Lund, Sweden. All spectra were collected in normal emission with an angular acceptance angle of ±6°. For C 1*s* and Pt 4*f*, we used photon energies of 390 and 190 eV, respectively. The spectra are normalized to the background, and core binding energies, defined to have positive values, are referenced to the Fermi edge. Accordingly, a positive core level shift (CLS) corresponds to a binding energy increase.

The Ir(111) crystal was cleaned by cycles of sputtering at room temperature and oxygen treatment at 1200 K followed by a short flash to 1400 K. A graphene layer was grown on Ir(111) by thermal decomposition of room-temperature adsorbed ethylene at 1420 K followed by 20 min ethylene exposure at 1120 to 1170 K at a pressure of 1×10^{-7} mbar.[17] We emphasize that this method and the use of sufficiently high temperatures for ethylene decomposition and graphene growth guarantee an entirely closed single layer, single orientation graphene film with an angular scatter $\Delta\varphi \approx 0.25^{\circ}$. Consequently, the film displays no graphene edge atoms and only a marginal concentration of point defects, which accommodate the small tilts. The quality of the graphene film was checked with low-energy electron diffraction (LEED), and the absence of CO adsorption at room temperature confirmed the full coverage of Ir(111) with graphene. Pt deposition was done with an *e*-beam evaporator calibrated on clean Ir(111) using the Ir $4f$ surface peak, which vanishes at 1 monolayer (ML) coverage. The XPS calibration was directly confirmed in Cologne with scanning tunneling microscopy (STM) by measuring the area of monolayer Pt islands grown on Ir(111) using the same evaporator at an identical distance. With an uncertainty of 10%, the two calibrations agreed. The STM data shown were also obtained in Cologne using the same sample preparation as for the XPS experiments.

Calculated core-level shifts reported herein were obtained in the fully screened hole approximation, in which the total energy of the system plus core hole is computed by setting the core potential of the ionized atom to that of the same atom with the appropriate core electron missing. Total energies were evaluated using the VASP DFT code,[18,19] with a local-density approximation (LDA) functional, based on the Ceperley-Alder local density functional,[20] as parametrized by,[21] in the projector augmented wave (PAW) approximation.[22,23] The LDA functional was chosen for the present work since it describes the binding of Ir islands on graphene better than the Perdew-Wang 1991 generalized gradient approximation (PW91-GGA) functional.[10]

As in [Ref. 10], we modeled graphene/Ir(111) as a 10×10 graphene adlayer on the upper surface of a 9×9, four-layer, Ir(111) crystalline slab. This is a very good approximation to the experimentally observed incommensurate 10.3×10.3 graphene layer on a 9.3×9.3 substrate mesh. In structural optimizations, with and without overlying Pt islands, the atoms of the bottom Ir layer were fixed in a (111) bulk, crystal plane, with an Ir-Ir nearest-neighbor distance equal to 2.701 Å, which is the theoretical optimum. Positions of all remaining atoms were relaxed until none experienced a force of magnitude >45 meV/Å. We accelerated electronic relaxation using Methfessel-Paxton Fermi-level smearing (width = 0.2 eV)[24] and corrected for the unphysical contact potential difference associated with having a graphene adlayer on only one side of the Ir slab.[25] We used a 400 eV plane-wave basis cutoff and a 3×3 surface Brillouin zone sample for the sake of good accuracy.

III. TEST CASE: CORE LEVEL SPECTRUM OF PRISTINE GRAPHENE ON Ir(111)

Figure 1(a) shows an STM topograph of graphene on Ir(111) with the moiré unit cell indicated. Both the honeycomb structure formed by the carbon atoms and the moiré's different high-symmetry domains are visible. The latter are labeled TOP, HCP, or FCC according to the position of the center of the carbon rings.[5] A ball model of the DFT optimized structure in Fig. 1(b) shows the geometry of the high-symmetry domains and the undulation of the graphene. C atoms in TOP domains reside 3.85 Å above the Ir surface, whereas those in HCP and FCC domains lie about 0.6 Å lower. The C atoms are grouped in Fig. 1(b) according to their height and binding geometry.

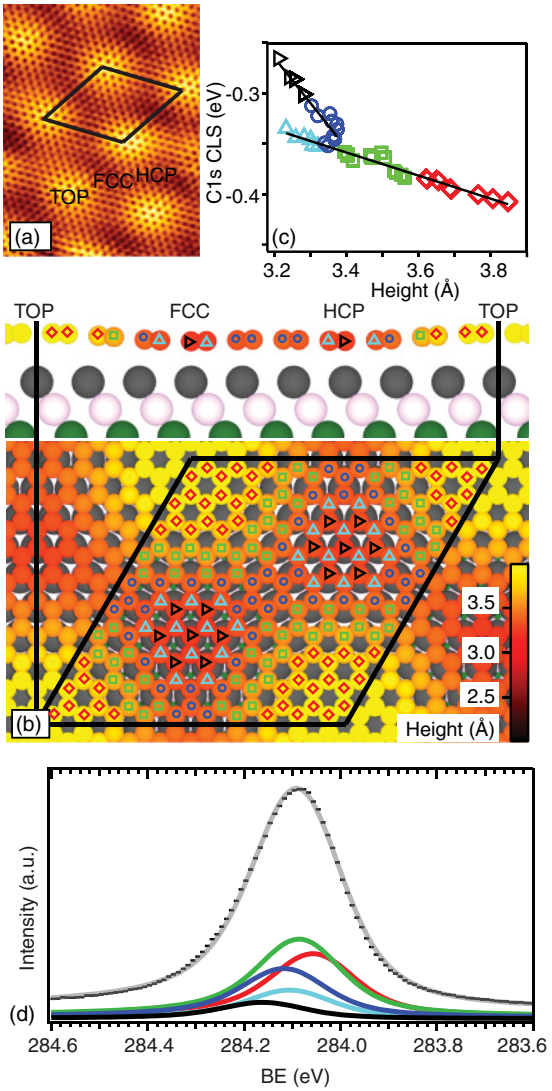

FIG. 1. (Color online) (a) STM topograph (59×84 Å^2, $U = 1$V, $I = 7$ nA) of the graphene moiré on Ir(111). The three high-symmetry domains TOP, FCC, and HCP are indicated. (b) Schematic of the DFT optimized C(10×10)/Ir(9×9) moiré unit cell showing a top view and a side view along the unit cell diagonal. The height of the C atoms is given by the color scale. The C atoms in threefold hollow sites are labeled by ◇ and △, in bridge sites by □, and in atop sites by ○ and ▷ (see text). (c) Calculated C 1*s* CLS for the 200 atoms in the moiré unit cell. (d) Black dots represent the experimental C 1*s* spectrum. The gray curve is the superposition of 200 peaks with a binding-energy distribution according to the DFT calculated CLS. The five colored components are the sums of peaks originating from C atoms marked with ◇, △, □, ○, and ▷ in panel (b).

Those in threefold hollow sites are labeled by ◇ and △, those in bridge sites by □, and those in atop sites by ○ and ▷.

To understand how the graphene-Ir(111) distance and the local geometry of C atoms affect the C 1*s* core level, we calculated the CLS of the 200 C atoms in the moiré unit cell using the core ionization potential of a C atom in an isolated graphene layer as a reference. The results are shown in Fig. 1(c) using the same colored symbols as in Fig. 1(b) to distinguish atoms at different heights and adsorption sites. Comparing C atoms in threefold hollow [◇ and △ in Figs. 1(b) and 1(c)] or bridge sites [□ in Figs. 1(b) and 1(c)] it is clear that there is an approximate linear correlation between the graphene-Ir(111) distance and the C 1*s* core level binding energy, which is lower for atoms farther from the substrate. Core shifts estimated in the initial-state approximation,[26] which are the main contributions to the numbers we calculated, offer insight into the sign of this effect. The key idea is that CLSs are more negative on atoms that gain electronic charge and more positive on those that lose it. Thus, the CLSs on C atoms farther from the metal imply that they are somewhat negatively charged, while the atoms that lie lowest are positive. This charge redistribution is consistent with an electrostatic interaction between the mobile electrons of the graphene and the electron spillout charge of the underlying metal. That is, the positive charge of the low-lying moiré regions is favorable by virtue of attraction to the metal's spillout electrons. Equally, the negative charge of the high-lying regions is favorable by virtue of repulsion from them.

Similarly to C atoms in threefold or bridge sites, we observe an approximately linear height to binding-energy (BE) correlation for C atoms positioned atop Ir atoms and marked with ○ and ▷ in Figs. 1(b) and 1(c). The slope, however, is a factor of four steeper for C atoms atop Ir (−0.45 eV/Å) compared to atoms in threefold or bridge sites (−0.11 eV/Å), consistent with a stronger interaction between C atoms' π orbitals and the $d_{3z^2-r^2}$ orbitals of the underlying Ir atoms for atop-positioned C atoms. This interaction seems a likely candidate for an explanation of why it is the HCP and FCC regions of the graphene film that lie low and not the TOP region. In the former, weak hybridization effects pull C atoms directly above Ir atoms toward the metal. In the TOP region, there are no C atoms directly above Ir atoms.[27,28]

Figure 1(d) shows the experimental C 1*s* spectrum obtained on pristine graphene/Ir(111). We observe a single C 1*s* peak at 284.09 eV with an experimental full width at half maximum (FWHM) of 0.25 eV. The experimental C 1*s* spectrum was fit with 200 peaks with identical intensity and C 1*s* CLSs according to our DFT calculations. Both the Gaussian and Lorentzian full width at half maximum (GFWHM and LFWHM, respectively) were constrained to one common fitting parameter for all 200 peaks during the fitting procedure. The result was a GFWHM and LFWHM of 0.15 and 0.12 eV, respectively. As shown by the gray curve in Fig. 1(d), the superposition of the 200 peaks is an excellent approximation to the experimental spectrum and the LFWHM is, furthermore, in good agreement with studies on HOPG.[29] To illustrate how atoms in different domains and adsorption sites contribute to the experimental spectrum, the C 1*s* sum spectrum of each of the five sets of atoms shown in Figs. 1(b) and 1(c) is included in Fig. 1(d).

The C 1*s* graphene/Ir(111) peak position of 284.09 eV measured here is similar to previously measured values of 284.16,[12] 284.10,[14] and 248.15 eV.[30] The measured experimental FWHM of 0.25 eV is lower than any reported value (0.40[12] and 0.30 eV[30]), consistent with the excellent quality of our graphene and the absence of defects and edge atoms. It is worth noting, incidentally, that because we only captured photoelectrons within an acceptance angle of ±6° about the surface normal, dispersion, such as was attributed in [Ref. 30] to formation of C 1*s* bands, cannot have contributed to the broadening of our C 1*s* XPS feature.

IV. C 1*s* CORE LEVEL SHIFTS OF GRAPHENE ON Ir(111) WITH Pt ADCLUSTERS

Satisfied that DFT calculations provide a faithful description of the C 1*s* spectrum of pristine graphene/Ir(111), we now wish to use them to test the rehybridization model of metal cluster array binding on the graphene. To that end, Fig. 2(a) shows an STM image obtained after room-temperature deposition of 0.18 ML Pt. The large majority of Pt clusters in the figure are one layer high, although a few bright two-layer islands are also apparent. All clusters are adsorbed in HCP domains, with the following occupation numbers: one-layered clusters (80 ± 2%), two-layered clusters (12 ± 2%), three-layered clusters (2 ± 1%), and empty cells (5 ± 1%). As, on average, 94% of the moiré unit cells contain a cluster, and each unit cell contains 87 Ir atoms,[5] the average Pt island is comprised of 17 atoms. Given an approximate Poisson size distribution,[5] clusters of size 15 to 19 atoms are all very similar in probability, ranging from 8.6 to 9.6%. Thus, to limit computational effort, we conducted DFT calculations for planar, highly symmetric, magic Pt19 clusters. As for Ir clusters supported by graphene,[10] our calculations imply that the Pt19 clusters are stabilized in HCP domains with the Pt atoms positioned atop C atoms. The optimized Pt19/graphene/Ir(111) structure is shown in Fig. 2(b). Comparison of the side view of pristine graphene in Fig. 1(b) and of graphene supporting Pt19 clusters in Fig. 2(b) shows that C atoms below and in the vicinity of the Pt19 cluster displace closer to the Ir(111) surface, while C atoms in TOP domains moved slightly away from the Ir surface (3.98 Å). Based on the observed height-BE correlation established for pristine graphene we expect a CLS to higher binding energies for the C atoms that have moved closer to the Ir(111) surface upon Pt deposition. The DFT-calculated C 1*s* CLS for the C atoms in the Pt19/graphene/Ir(111) structure, shown in Fig. 2(c), confirm the expected positive CLS below and in the vicinity of the Pt19 cluster.

In more detail we find that the C atoms surrounding the Pt-cluster [○ in Fig. 2(c)] have a linear BE-height correlation with an even steeper slope (−1.6 eV/Å) than for pristine graphene (−0.11 eV/Å threefold hollow and bridge, −0.45 eV/Å atop). Coordination directly to Pt atoms (◇) adds an additional CLS of +0.6 eV on top of the CLS expected from the C-Ir(111) distance, while C atoms atop Ir atoms (▽) below the Pt19 cluster have an extra CLS of −0.5 eV. As the observed negative and positive shifts are approximately equal in magnitude, Pt deposition evidently leads to charge transfer of electrons from Pt-bonded C atoms to Ir-bonded C atoms below the Pt clusters

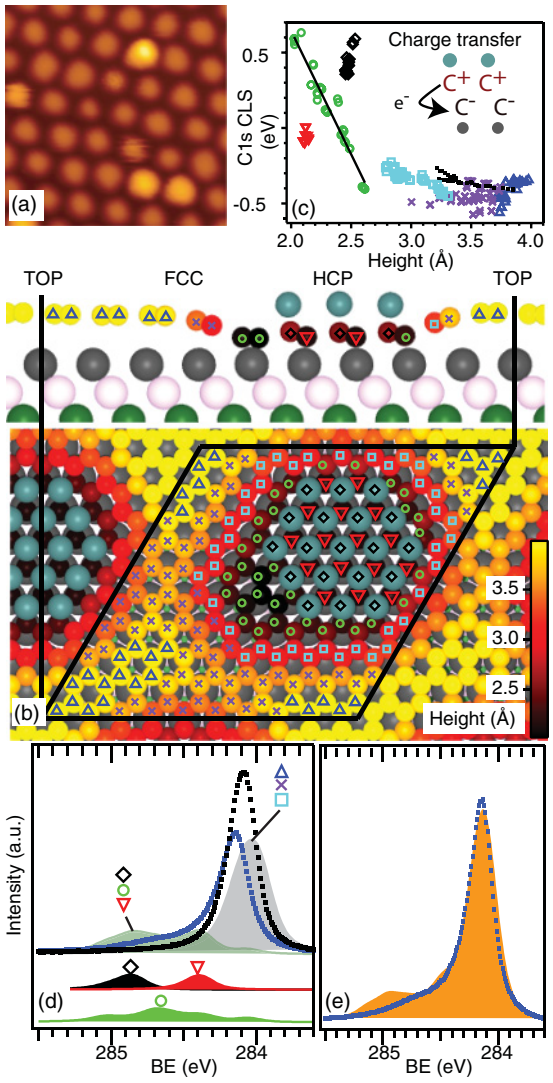

FIG. 2. (Color online) (a) STM topograph ($U = 1$V, $I = 0.05$ nA, 150×150 Å^2) after deposition of 0.18 ML Pt on graphene. (b) Schematic of the DFT optimized C(10 × 10)/Ir(9 × 9) moiré unit cell with an adsorbed Pt19 cluster showing the top view and the side view along the unit cell diagonal. The height of the C atoms is given by the color scale. C atoms are grouped into 6 sets based on their position in the moiré unit cell (◇, ▽, ○, □, ×, and △). (c) Calculated C 1*s* CLS for the atoms in graphene supporting a Pt19 cluster. Symbols used as in panel (b). The shift is given relative to a C atom in isolated graphene. The black dots are the data of pristine graphene as in Fig. 1(c). (d) Experimental C 1*s* spectrum before (black dots) and after (blue dots) deposition of 0.18 ML Pt. The curves marked with (◇), (▽), and (○) symbols are the DFT calculated components corresponding to Pt-bonded C atoms, Ir-bonded C atoms, and C atoms close to the Pt19 cluster, respectively. The light gray and light green curves are the DFT calculated C 1*s* component of atoms far away from and close to the Pt cluster, respectively. (e) Comparison of the experimental C 1*s* spectrum after deposition of 0.18 ML Pt and the overall DFT simulated spectrum shifted +0.1 eV and corrected for attenuation of the photoelectrons (see text).

[see the small schematic in Fig. 2(c)]. Based on the DFT calculations, the Pt clusters' effect on the C 1*s* CLS is therefore twofold: (i) The polarization of charge, toward the Ir substrate as C-Ir bonds form, increases the average C 1*s* CLS. (ii) The $sp^2 \rightarrow sp^3$ rehybridization induces a transfer of electrons from Pt-bonded C atoms to Ir-bonded C atoms.

Toward confirming that our Pt19 model and the $sp^2 \rightarrow sp^3$ rehybridization are faithful to nature, let us compare the DFT and measured C 1*s* spectra after deposition of 0.18 ML Pt in Fig. 2(d). Relative to the C 1*s* spectrum of pristine graphene, shown with black dots, Pt deposition shifts the main peak by +0.06 eV (blue dots), while a broad shoulder develops at high binding energies. Comparing with Figs. 2(b) and 2(c), we identify the shoulder with three groups of C atoms: immediate neighbors of Pt atoms (◇), contributing CLS in a width of 0.24 eV, immediate neighbors of Ir atoms (▽), with CLS covering 0.10 eV, and C atoms bordering the Pt island (○), with CLS ranging over 1.04 eV. Using the peak shape from pristine graphene and the C 1*s* CLS from DFT we calculated the C 1*s* peak originating from each of the 200 C atoms in a graphene unit cell supporting a Pt19 cluster. Furthermore, we used these calculated C 1*s* peaks as input to calculate the shape of the 3 components assigned to the experimental shoulder. As Fig. 2(d) shows, the addition of these three components (◇, ▽, ○) results in a broad shoulder largely matching the experimental one in width.

Still, the overall intensity of the simulated shoulder is too high, particularly the component with the highest binding energies, from C atoms directly bound to Pt cluster atoms [marked ◇ in Figs. 2(b)–2(d) and component shaded black in Fig. 2(d)]. The overestimate of the overall intensity of the shoulder in the calculated spectrum is a likely consequence of the attenuation of the photoelectron signal originating from C atoms below the Pt19 clusters. In fact, attenuation of the calculated shoulder components by 40%—the attenuation of one layer of Pt in the Pt(111) surface at $E_{\mathrm{kin}} = 390$ eV − 284 eV = 106 eV—brings the overall intensity to reasonable match with experiment [see below and Fig. 2(e)]. Furthermore, we find that the area of the experimental shoulder is increased by a factor of 1.3 when the C 1*s* spectrum is acquired with $h\nu = 390$ eV compared to spectra taken with $h\nu = 350$ eV and $h\nu = 450$ eV, indicating that diffraction effects are important for the shoulder area at low kinetic energy of the photoelectrons. The area of the shoulder component is, however, increased again when the C 1*s* spectrum is measured with $h\nu = 500$ eV and $h\nu = 600$ eV. At high kinetic energy of the photoelectron, attenuation and diffraction effects will be less important and we are, therefore, unable to explain the overweighting of the high-binding-energy shoulder ["discrepancy (A)" in what follows].

Addition of the remaining calculated components (□, ×, △) results in a *negative* shift for the main peak upon cluster adsorption, as the gray curve in Fig. 2(d) demonstrates. This calculated negative shift of the main component contradicts its experimentally observed positive shift by 0.06 eV ["discrepancy (B)" in the following discussion].

Although calculations and experiment agree on the formation of a high-energy binding-energy shoulder in the C 1*s* CLS upon cluster adsorption, the sources of discrepancies (A) and (B) are, given current knowledge, a matter of speculation. For example, a minute difference between actual and calculated doping might account for discrepancy (B). Such a difference could result from neglect of the cluster size distribution in our

calculations. Indeed, it was recently observed in photoemission spectroscopy that Ir cluster adsorption on graphene on Ir(111) shifts graphene's π conduction band.[31] By hand, on that basis, we shifted all theoretical peaks by +0.1 eV and additionally scaled down the shoulder components by 40% to account for photoelectron attenuation by the Pt19 clusters. The resulting spectrum, shaded orange in Fig. 2(e), is a reasonable match to the experimental one. Nonetheless, discrepancy (A) remains.

According to the correlation we have established between C-atom height and C 1s binding energy, excess weight theoretically attributed to the highest binding energy peak [discrepancy (B)] means that in the region between the Pt islands, the graphene sheet lies too close to the underlying Ir substrate. Given the tendency of the LDA to overbind, it is easy to imagine that a more faithful density functional would mitigate this problem. Still, for graphene/Ir(111) with no island present, the predicted C 1s spectrum agrees well with experiment (cf. Fig. 1). Thus, a geometric solution of discrepancy (B) is not straightforward, and the answer may lie entirely elsewhere.

V. Pt 4f CORE LEVEL SHIFTS OF Pt CLUSTERS ADSORBED ON GRAPHENE/Ir(111)

For separate confirmation that our Pt19 model and the $sp^2 \rightarrow sp^3$ rehybridization describe the experimentally observed situation correctly, we compared the DFT-calculated CLS of Pt 4f with the experimental spectrum. Figure 3(a) shows the calculated Pt 4$f_{7/2}$ CLS of the 19 Pt atoms in the cluster using the CLS of a Pt bulk atom as reference with a known BE of 70.9 eV.[32] Our calculations show that

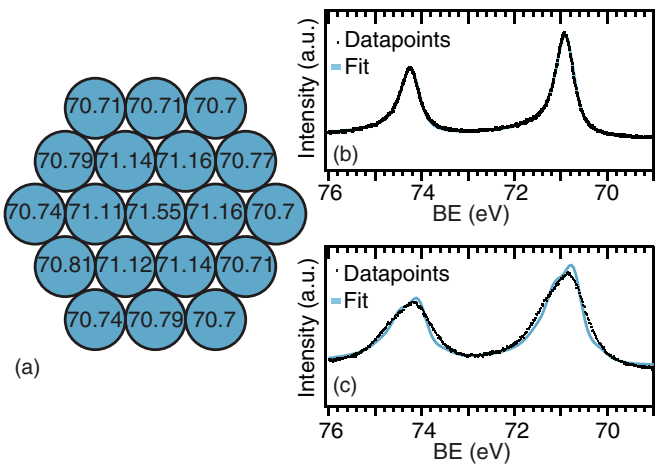

FIG. 3. (Color online) (a) Calculated Pt 4$f_{7/2}$ core levels for the Pt19 cluster. The atomic configuration used to calculate the Pt 4$f_{7/2}$ core levels is identical to Fig. 2(b). (b) Experimental Pt 4f spectrum (dots) of monolayer Pt islands (0.5 ML) adsorbed on a clean Ir(111) surface. The light blue line shows the result of the curve fitting, when one Pt 4$f_{7/2}$ component and one Pt 4$f_{5/2}$ component were used. (c) Experimental Pt 4f spectrum (dots) of 0.18 ML Pt deposited onto graphene. The light-blue curve is the result of the curve fitting, with CLS fixed to the DFT calculated values in (a), and the LFWHM and GFWHM fixed to the values for Pt adsorbed on clean Ir (111).

the Pt atoms at the perimeter of the cluster have Pt 4$f_{7/2}$ CLS of −0.1 to −0.2 eV relative to bulk Pt, while the six atoms surrounding the central atom have an additional shift of ∼0.4 eV and the central Pt atom has an additional shift of ∼ 0.8 eV.

To understand the significance of these CLSs, in a first experiment we have grown 0.5 ML Pt at 580 K directly on Ir(111). At this coverage and temperature Pt forms monolayer islands with the large majority of the Pt atoms six-fold coordinated to Pt and three -fold coordinated to the Ir(111) substrate.[6] Figure 3(b) displays the experimental Pt 4f spectrum. We deconvoluted the experimental spectrum with one single Pt 4$f_{7/2}$ and Pt 4$f_{5/2}$ component. The curve fitting reveals that the Pt 4$f_{7/2}$ component has a binding energy of 70.88 eV, a GFWHM (0.29 eV), and LFWHM (0.31 eV).

Figure 3(c) displays the experimental Pt 4f spectrum of 0.18 ML Pt deposited onto graphene. The Pt peaks are much broader than for Pt deposited onto clean Ir(111). To test if our DFT calculated CLS are able to explain the observed peak broadening we fit the experimental Pt 4f spectrum of Pt/graphene with 19 Pt 4$f_{7/2}$ and 19 Pt 4$f_{5/2}$ components with similar intensities and binding energies fixed to the DFT calculated values. Furthermore, the GFWHM and LFWHM were fixed to the values obtained for Pt adsorbed on clean Ir(111) during the fitting procedure. The light blue curve in Fig. 3(c) shows the result of the curve fitting. It is apparent that the experimental broadening of the Pt 4f peaks is well reproduced by the DFT calculated CLS. Also, the absolute DFT-calculated binding energy positions of the Pt 4f components match excellently with the experimental spectrum. The only discrepancy between the experimental Pt 4f spectrum and the fit is that the overall width of Pt 4f peaks in the fit is slightly too small. If the GFWHM is increased from 0.29 to 0.6 eV during the fitting procedure the fit reproduces the experimental curve almost perfectly. An increased GFWHM could be the result of less symmetric clusters, the experimental cluster size distribution, and a larger vibrational broadening of Pt/graphene than on Pt/Ir(111).

VI. CONCLUSIONS

In summary, we have demonstrated a linear correlation between C-atom height and 1s binding energy in a graphene adlayer on Ir(111), reflecting an electron charge redistribution consistent with the adlayer's undulation geometry. Upon deposition of 0.18 ML Pt we observed by STM well-ordered, single-layer clusters in the graphene HCP domains. The corresponding changes in XPS spectra submitted to an interpretation based on DFT modeling of the clusters as highly symmetric, flat, and comprised of 19 Pt atoms. Specifically, a broad C 1s shoulder develops upon Pt deposition and, using DFT-calculated CLS, we showed that this shoulder must be assigned to C atoms under and in the vicinity of the Pt cluster. More detailed calculations revealed that the $sp^2 \rightarrow sp^3$ rehybridization further broadens the shoulder because of electron transfer from Pt-bonded C atoms to Ir-bonded C atoms. However, the calculations imply a larger weight of the highest binding energy component and a slight positive shift of the main component of the C 1s CLS relative

to experimental observation. Of considerable interest would be to learn whether these discrepancies are attributable to limitations of our physical model (i.e., assuming clusters of just one size and shape) or to systematic error in our DFT implementation. Lastly, we compared measured and calculated Pt $4f_{7/2}$ CLSs and found an excellent agreement, offering a solid starting point for future gas-adsorption studies. In particular, the CLS of the edge atoms of the Pt19 clusters are shifted -0.4 eV with respect to terrace atoms affording the opportunity to distinguish step- and terrace-site adsorption.

ACKNOWLEDGMENTS

Financial support by Deutsche Forschungsgemeinschaft (MI581/17-2), the Swedish Research Council, and the Danish Council for Independent Research is gratefully acknowledged. Work by P. J. F. was supported by the US DOE Office of Basic Energy Sciences, Division of Materials Sciences and Engineering, under Contract No. DE-AC04-94AL85000. Sandia is operated by the Lockheed Martin Co. for the US Department of Energy's National Nuclear Security Administration under contract DE-AC04-94AL85000. Support by the MAX IV Laboratory staff is also gratefully acknowledged.

*jan.knudsen@sljus.lu.se

[1] Y. Pan, M. Gao, L. Huang, F. Liu, and H.-J. Gao, Appl. Phys. Lett. **95**, 093106 (2009).
[2] K. Donner and P. Jakob, J. Chem. Phys. **131**, 164701 (2009).
[3] Z. Zhou, F. Gao, and D. W. Goodman, Surf. Sci. **604**, L31 (2010).
[4] M. Sicot, S. Bouvron, O. Zander, U. Rüdiger, Y. S. Dedkov, and M. Fonin, Appl. Phys. Lett. **96**, 093115 (2010).
[5] A. T. N'Diaye, S. Bleikamp, P. J. Feibelman, and T. Michely, Phys. Rev. Lett. **97**, 215501 (2006).
[6] A. T. N'Diaye, T. Gerber, C. Busse, J. Mysliveček, J. Coraux, and T. Michely, New J. Phys. **11**, 103045 (2009).
[7] R. Balog, B. Jørgensen, L. Nilsson, M. Andersen, E. Rienks, M. Bianchi, M. Fanetti, E. Lægsgaard, A. Baraldi, S. Lizzit, Z. Sljivancanin, F. Besenbacher, B. Hammer, T. G. Pedersen, P. Hofmann, and L. Hornekær, Nat. Mater. **9**, 315 (2010).
[8] M. L. Ng, R. Balog, L. Hornekær, A. B. Preobrajenski, N. A. Vinogradov, N. Mårtensson, and K. Schulte, J. Phys. Chem. C **114**, 18559 (2010).
[9] S. Barja, M. Garnica, J. J. Hinarejos, A. L. Vázquez de Parga, N. Martin, and R. Miranda, Chem. Commun. **46**, 8198 (2010).
[10] P. J. Feibelman, Phys. Rev. B **77**, 165419 (2008).
[11] P. J. Feibelman, Phys. Rev. B **80**, 085412 (2009).
[12] A. B. Preobrajenski, M. L. Ng, A. S. Vinogradov, and N. Mårtensson, Phys. Rev. B **78**, 073401 (2008).
[13] E. Miniussi, M. Pozzo, A. Baraldi, E. Vesselli, R. R. Zhan, G. Comelli, T. O. Mentes, M. A. Nino, A. Locatelli, S. Lizzit, and D. Alfe, Phys. Rev. Lett. **106**, 216101 (2011).
[14] P. Lacovig, M. Pozzo, D. Alfè, P. Vilmercati, A. Baraldi, and S. Lizzit, Phys. Rev. Lett. **103**, 166101 (2009).
[15] Z. Sun, S. K. Hämäläinen, J. Sainio, J. Lahtinen, D. Vanmaekelbergh, and P. Liljeroth, Phys. Rev. B **83**, 081415 (2011).
[16] R. Nyholm, J. N. Andersen, U. Johansson, B. N. Jensen, and I. Lindau, Nucl. Instrum. Methods Phys. Res., Sect. A **467**, 520 (2001).
[17] R. van Gastel, A. T. N'Diaye, D. Wall, J. Coraux, C. Busse, N. M. Buckanie, F.-J. Meyer zu Heringdorf, M. Horn von Hoegen, T. Michely, and B. Poelsema, Appl. Phys. Lett. **95**, 121901 (2009).
[18] G. Kresse and J. Furthmüller, Comput. Mater. Sci. **6**, 15 (1996).
[19] G. Kresse and J. Furthmüller, Phys. Rev. B **54**, 11169 (1996).
[20] D. M. Ceperley and B. J. Alder, Phys. Rev. Lett. **45**, 566 (1980).
[21] J. P. Perdew and A. Zunger, Phys. Rev. B **23**, 5048 (1981).
[22] P. E. Blöchl, Phys. Rev. B **50**, 17953 (1994).
[23] G. Kresse and D. Joubert, Phys. Rev. B **59**, 1758 (1999).
[24] M. Methfessel and A. T. Paxton, Phys. Rev. B **40**, 3616 (1989).
[25] J. Neugebauer and M. Scheffler, Phys. Rev. B **46**, 16067 (1992).
[26] W. F. Egelhoff Jr., Surf. Sci. Rep. **6**, 253 (1986).
[27] E. Starodub, A. Bostwick, L. Moreschini, S. Nie, F. E. Gabaly, K. F. McCarty, and E. Rotenberg, Phys. Rev. B **83**, 125428 (2011).
[28] C. Busse, P. Lazic, R. Djemour, J. Coraux, T. Gerber, N. Atodiresei, V. Caciuc, R. Brako, A. T. N'Diaye, S. Blügel, J. Zegenhagen, and T. Michely, Phys. Rev. Lett. **107**, 036101 (2011).
[29] T. Balasubramanian, J. N. Andersen, and L. Walldén, Phys. Rev. B **64**, 205420 (2001).
[30] S. Lizzit, G. Zampieri, L. Petaccia, R. Larciprete, P. Lacovig, E. D. L. Rienks, G. Bihlmayer, A. Baraldi, and P. Hofmann, Nat. Phys. **6**, 345 (2010).
[31] S. Rusponi, M. Papagno, P. Moras, S. Vlaic, M. Etzkorn, P. M. Sheverdyaeva, D. Pacilé, H. Brune, and C. Carbone, Phys. Rev. Lett. **105**, 246803 (2010).
[32] O. Björneholm, A. Nilsson, H. Tillborg, P. Bennich, A. Sandell, B. Hernnäs, C. Puglia, and N. Mårtensson, Surf. Sci. **315**, L983 (1994).